

APPLICATION OF SMALL-ANGLE X-RAY SCATTERING (SAXS) VIA SYNCHROTRON RADIATION FOR STRUCTURAL ANALYSIS OF SEMI-CRYSTALLINE POLYMER: STUDY CASES FROM POLYPROPYLENE FOR INDUSTRIAL USAGE

Wonchalerm Rungswang*, Chatchai Jarumaneeroj, and Vadee Chivatana-soontorn

Received: June 18, 2015; Revised: August 06, 2015; Accepted: August 07, 2015

Abstract

Among advanced techniques for structural analyses of polymer, X-ray scattering via a synchrotron source is the prominent one which contributes to fundamental findings in polymer science. The small-angle X-ray scattering technique can be used to reveal the polymers' structures in detail, from the radius of the gyration of polymer chains in a molten state to lamellar crystal in a solidified state. Here, those structural analyses via *in-situ* synchrotron radiation experiments were reviewed by using commercial polypropylene as study cases for industrial research.

Keywords: Synchrotron radiation, SAXS, polypropylene, crystal structure

Introduction

Since the 1920s when Hermann Staudinger proposed the concept of the macromolecule and polymer structure, numerous attempts have been devoted to clarifying the structures of polymers which definitely correspond to their properties (Mülhaupt, 2004). Chemical structure, which is the basic information for identifying the type of polymers, can be classified by conventional analytical techniques, such as infrared (IR) spectrometry and nuclear magnetic resonance (NMR) (Putzig *et al.*, 1994; Busico *et al.*, 2002). In more detail, the structure of the polymer chain can be identified as a physical arrangement of its chain or branching, the so-called microstructure,

and this always play an important role in the polymer's properties (Busico and Cipullo, 2001; Rungswang *et al.*, 2012; Stadler and Karimkhani, 2011). The characterization of the microstructure is complicated, especially for polyolefins which consist of only carbon and hydrogen atoms. Combining advanced techniques, such as gel permeable chromatography (GPC) with multi-detectors and rheological measurement with complicated mathematic models, is the way to trace that structure in depth (Stadler and Mahmoudi, 2013; Yau, 2005). However, the polymeric system is more complicated when the assembly of the polymer chains is considered.

SCG Chemical Co., Ltd., Siam Cement Group (SCG). 101-1 Road, Map Ta Phut Industrial Estate, Muang District, Rayong Province 21150, Thailand. E-mail: wonchalr@scg.co.th

* Corresponding author

The polymeric chains are thermodynamically favored to form the supra-structures, for which the dimension is in the range from tens of nanometers to a few millimeters. The crystal structure is the familiar criterion which is the key factor for controlling the mechanical properties of polymeric products, such as strength and stiffness. It is important to note that polymers containing both crystalline and amorphous structures are classified as semi-crystalline polymers, such as polyethylene (PE) and polypropylene (PP). The hierarchical structure of the polymer crystalline can be as depicted in Figure 1. The chains are uniformly packed in the crystal lattice with a specific crystal type, and the lattices are formed into the stacked lamellar structure. Without disturbance the polymer melts during its crystallization, the lamellar crystals grow radially from the nucleus to form a micrometer-scale spherical structure, called spherulite (Peacock, 2000; Galeski, 2003; Alexander, 1969).

In the research field of the polymer structure-property relationship, those supra-structures have been the main focus and have been studied in depth with various advanced techniques having been applied. Among those techniques, X-ray scattering is considered as an effective and extensive one due to a matching of the X-ray wavelength with the structural dimension (Piorkowska and Rutledge, (2013). Small-angle X-ray scattering (SAXS) is normally employed to probe the polymer structures, such as the radius of gyration (R_g) and thickness of the lamellar crystal for which the

dimensions are in the nanometer range. However, it is important to note that the key to the X-ray scattering techniques is the quality of the X-ray source. For common laboratory-scale instruments, the intensity of the X-ray is relatively low, and this is a major obstruction for advanced studies, for example, studying the failure mechanism for which an *in-situ* experiment is required. The structural evolution is measured while the polymer specimen is under macroscopic change, such as tensile deformation, shear, and modulated temperature.

Synchrotron radiation is a promising source of an intense X-ray; its flux is far higher than that of laboratory-scale X-ray source instruments, and this significantly extends the capability for polymer research (Roe, 2000). Several detailed structures have been revealed for the first time. For example, Wasanasuk *et al.* (2011) reported the most precise structure of poly (L-lactic) acid by using the high-energy synchrotron (SPring-8, Japan) for the X-ray diffraction analysis. Moreover, advanced studies, especially *in-situ* experiments, have been successfully done. For instance, the structural evolution of PP can be traced every 2-3 seconds under isothermal treatment, and this reveals in detail the mechanism of the structural change from the melt to the crystal structure (Reddy *et al.*, 2009).

Here, SAXS experiments and analyses of the semi-crystalline polymer via intense X-ray from a synchrotron source are reviewed through study cases of PP which is a good example for studying the semi-crystalline polymer. Several

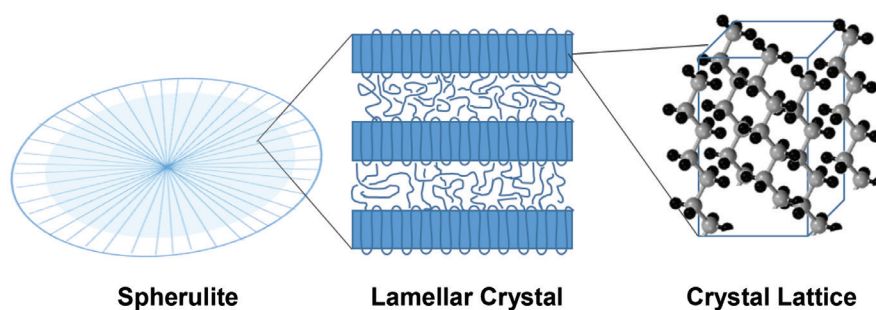


Figure 1. Hierarchical structure of polymer crystal

analyses were shown to evaluate the detailed structure in both the melt and solid states with the *in-situ* studies, especially for the industrial uses.

Results and Discussion

Polymer in the State

Above the melting temperature (T_m), the polymer chains are in a random coil configuration occupying in space. Its size can be quantitatively measured as a radius of the polymer coil referring to the center of mass (CM) and the radius of gyration (R_g) the mathematical description of which is shown below in Equation (1) (Rubinstein and Colby, 2003):

$$R_g^2 = \frac{1}{N} \sum_{i=1}^N (\vec{R}_i - \vec{R}_{CM})^2 \quad (1)$$

where \vec{R}_i and \vec{R}_{CM} are the position vectors of the i th monomer and the CM of the polymer chain, respectively.

The R_g can be determined by SAXS in the region governed by Guinier's law (Equation 2) which is calculated from the slope of $\ln[I(q)]$ and the q^2 plot. It should be noted that Guinier's law is limited to the small q region which is in the range of $q \cdot R_g < 1.3$ (Roe, 2000).

$$\ln[I(q)] = \ln[I(0)] - \frac{q^2 R_g^2}{3} \quad (2)$$

At an elevated temperature, the polymer chains tend to expand if the time period is long enough. For example, PP was heated in the heating chamber at 200°C, at which its T_m is about 160°C. The *in-situ* SAXS was measured to trace the change of the R_g , as shown from unpublished data in Figure 2. The result shows that the R_g linearly increases with time from ~7.5 nm to ~9.3 nm in 35 minutes. This suggests that the polymer chain continuously expands during the isothermal treatment. It might reach the equilibrium state in a certain period of time but the result indicates that a period of 35 minutes is too short for equilibration in this case.

Apart from the homogeneous phase mentioned earlier, the SAXS study can also be

extended to the hetero-phase system, such as a polymer blend. Normally, PP is rigid which limits its usage to only a few applications. Thus, blending with rubber or tough polymers is one of the approaches to toughen PP for diverse uses. However, the deteriorated phase-separation between the PP matrix and the rubber, and the cost are the major concerns. This leads to the development of sequential polymerization technology. Two-type reactors with a series design and specific catalytic system are affordable means to produce the multiphase polymer, or polymer alloy. The homo-PP is mainly produced in the first reactor as the matrix. The rubber, which is a random copolymer of 1-alkene and propylene, normally ethylene-propylene rubber (EPR), is produced as a minor phase in the second reactor. This in-reactor blend, which gives superior impact resistance due to the small size and good dispersion of the rubber phase, is called impact-resistant PP copolymer (IPC) (Zhu *et al.*, 2008). However, a dramatic increase of the rubber size is usually observed when the IPC is heated above its T_m for a certain period of time. Figure 3(A) and 3(B) shows the SEM micrographs of the xylene-etched IPC samples in which the craters observed on the samples' surfaces indicate the presence of the EPR's size and shape. Indirect evidence can be revealed by the SAXS with the *in-situ* heating chamber, as mentioned earlier. In this case, the Debye-Bueche model shown in Equation (3) for a two-phase system with their proximate refractive indices is used to evaluate the correlation length (ζ) of the adjacent PP domains (Reddy *et al.*, 2009; Rungswang *et al.*, 2013).

$$\frac{1}{I(q)} = \left[\frac{1}{A} + \left(\frac{\zeta^2}{A} \right) \cdot q^2 \right]^2 \quad (3)$$

where A is a constant, and ζ is determined from the slope and intercept of the $I(q)^{-1/2} - q^2$ plot. The agglomeration of the EPR phase in the melt, at 200°C, can be observed as the increasing of ζ as a function of time, shown in Figure 3(C), which is relevant to the SEM result in Figure 3(A) and 3(B). It is important to note that the size of the EPR droplet directly affects the impact resistance

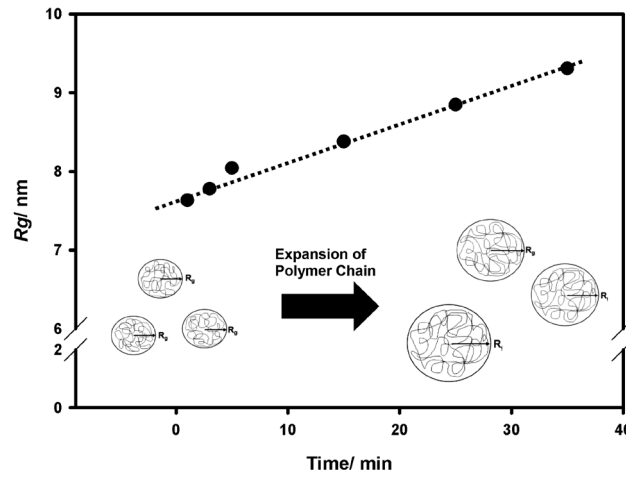


Figure 2. Radius of gyration (R_g) of PP melt measured by SAXS with isothermal treatment at 200°C in various times including schematic illustrating polymer-chain expansion (unpublished data) (Rungswang *et al.*,)

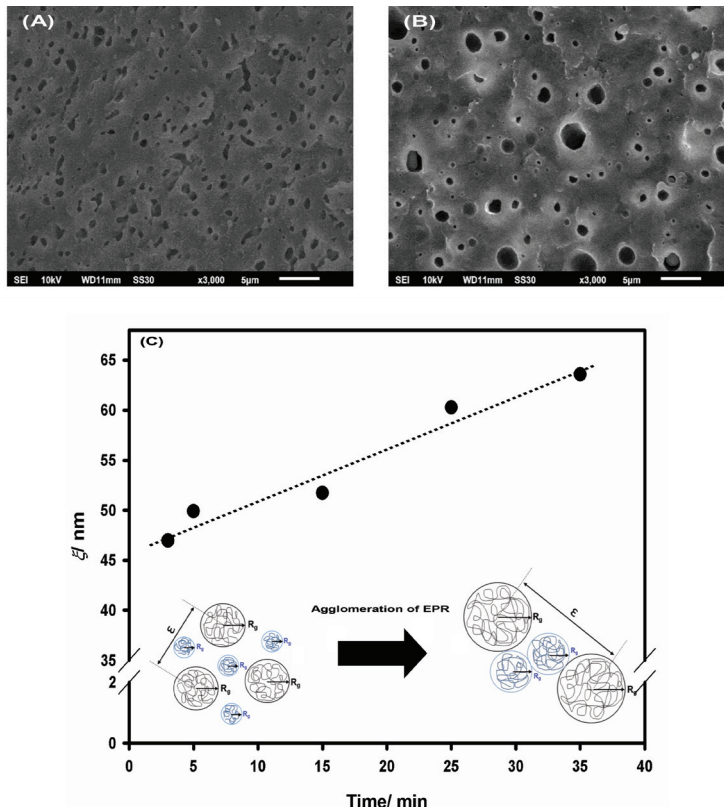


Figure 3. SEM images of xylene-etched IPC specimens (A) before and (B) after annealing at 200°C for 30 minutes, and correlation length (ζ) of IPC melt measured by SAXS with isothermal treatment at 200°C in various times including schematic illustrating EPR agglomeration (unpublished data) (Rungswang *et al.*,)

of the IPC product. Thus, this result makes the point that attention needs to be paid to controlling the resident time and temperature during the melt processing, especially in long time processing such as the rotomolding process.

Polymer in Solid State

As mentioned previously, the polymer crystal is formed below the crystallization temperature (T_c) as the support structure for strengthening the material. To understand the role of the crystallite on the material's failure and its mechanism, the focus is on the *in-situ* experiment for the mechanical test with an X-ray scattering measurement. For the injection specimen which is the common processing for PP product, the orientation of the lamellar crystal is a critical factor to manipulate the end-product's properties. Shepard *et al.* (1997) have reported the

effect of the lamellar orientation on the uniaxial tensile properties of the IPC. The specimens were prepared by compressing the injected IPC sheet at 200°C so that it is thin enough to cut into dog-bone specimens in the injection (ID-IPC) and transverse-injection (TD-IPC) directions, as shown in Figure 4. Then, the specimens were uniaxially stretched in the stretching direction (SD) with the *in-situ* SAXS measurements. The SAXS patterns of the unstretched specimens clearly show, in Figure 4, a two-point pattern indicating a fibril structure with the alternation of the lamellar crystal and amorphous layer. The orientation of the crystallite can be clearly seen from the SAXS patterns which indicate that the normal vectors of the lamella (n_L) and the fibril (n_F) are oriented perpendicular and parallel to the SD, respectively, for ID-IPC. Thus, the TD-IPC is, of course, in the opposite direction. The

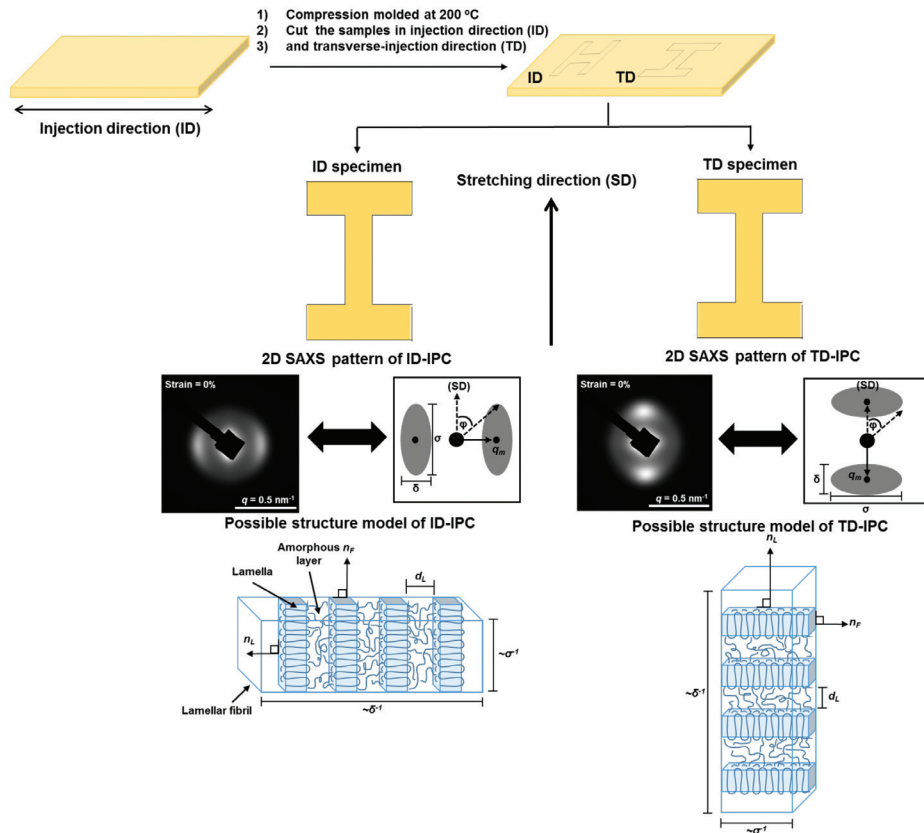


Figure 4. Schematic draw illustrating preparation of TD-IPC and ID-IPC specimens including SAXS patterns and possible model in real space (Rungswang *et al.*,)

orientation of the lamella can be quantitatively analyzed by Herman’s orientation function, as shown in Equations 4 and 5.

$$f = \frac{[3\langle \cos^2 \varphi \rangle - 1]}{2} \tag{4}$$

$$\langle \cos^2 \varphi \rangle = \frac{\int_0^\pi I_{(\varphi)} \cos^2 \varphi \sin \varphi d\varphi}{\int_0^\pi I_{(\varphi)} \sin \varphi d\varphi} \tag{5}$$

where φ is the azimuthal angle which is set to zero in the meridional direction or SD. The f is the unity for the n_L perfectly oriented perpendicular to the SD, while it is -0.5 for the

n_L perfectly oriented parallel to the SD. In case of random orientation, the f is close to zero.

Figure 5 clearly reveals that the TD-IPC shows better resistance to the uniaxially tensile deformation, i.e. elongation and strength at break, than that of the ID-IPC. The SAXS patterns of both the TD-IPC and ID-IPC series clearly show the evolution of the crystallite during the stretching. To trace the structure change in detail, several parameters were evaluated from the SAXS pattern, as shown in Figure 4. The lamellar repeating period (d_L) was calculated from the magnitude of the q vector at the maximum intensity (q_{max}) ($d_L = 2\pi/q_{max}$). The peak widths, i.e. σ and δ , of the two-point pattern are reciprocal to the

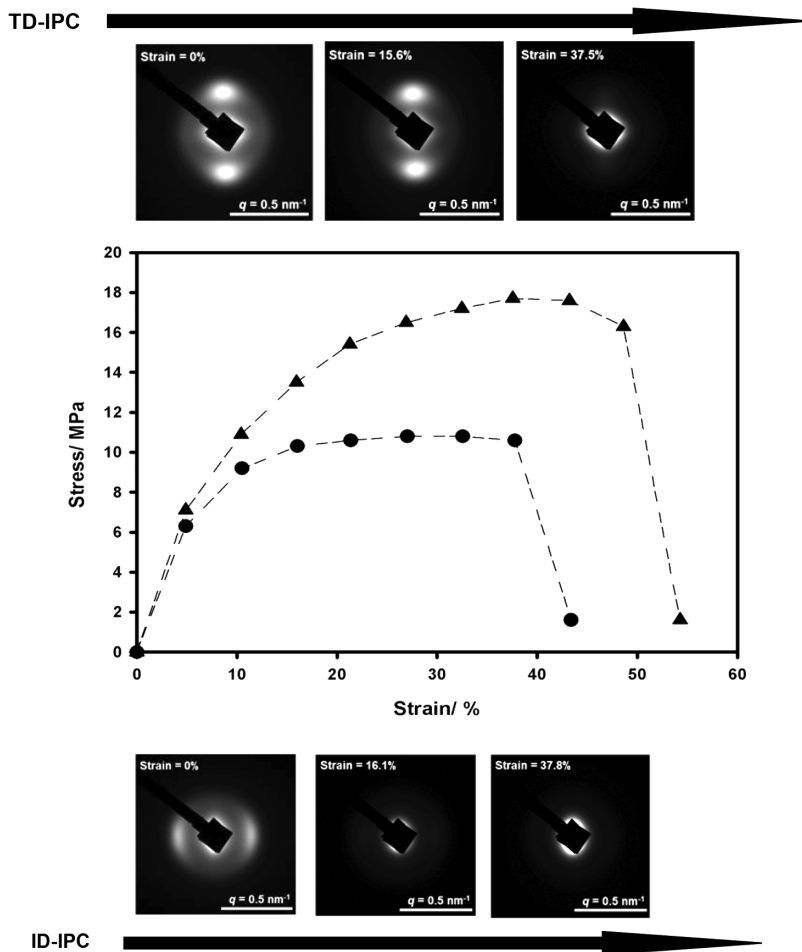


Figure 5. Tensile stress-strain curves, and SAXS patterns at specific strain of TD-IPC (●) and ID-IPC (▲) (Rungswang *et al.*,)

widths of the fibril lamella, as depicted in Figure 4. Furthermore, the number of the lamellae in each fibril (m) can be estimated by the following Equation 6:

$$m = kq_m(\sigma^{-2} + \delta^{-2})^{1/2} \cdot \cos\left[\alpha + \tan^{-1}\left(\frac{\delta}{\sigma}\right) - \frac{\pi}{2}\right] \quad (6)$$

where α is the angle between n_L and n_F , and k is the constant which is simply set to be a unity. The detail of the study was clearly verified in the original work (Rungswang *et al.*, 2013). However, the conclusion with the proposed mechanism is shown in Figure 6. In the case of the TD-IPC, due to the orientation of the fibril with its n_F perpendicular to the SD, the fibril was elongated when it was stretched, as evidenced by the decreasing of the peak width δ . The d_L values are increased with the increasing strain which indicates that the lamellar repeating period is widened. It is in contrast to the ID-IPC. The dramatic reduction of the m values and increase of both peak widths σ and δ with stretching suggests the dominance of the fibril-fragmentation mechanism, and this is the reason for the worse tensile properties in the ID-IPC. This study is important for an injection molding product in which the orientation of the crystallite is one

of the keys for controlling the mechanical properties. This leads to the important question of how the crystal orientation, including its structure, can be specifically controlled.

The addition of additives, such as a nucleating agent (NA) and clarifying agent, is one approach to manipulate the crystal structure which is normally used in industry due to its effectiveness with simple modifications and low cost. The crystal size is a direct consequence of the NA resulting in controlling the product's appearance. For example, sorbitol-based NA induces a very small crystal, and this yields high transparency of the PP product. It is important to note that the sorbitol-based NA can be dissolved in a PP melt at a high temperature (processing temperature) and recrystallized above its T_c . A tiny crystal of the NA with a rod-like shape forms, and induces the PP crystal with a small size compared with other NAs (van der Meer, 2003).

The crystal phase can also be modified by the NA. It is well known that 3 crystal phases are found in PP, i.e. α , β , and γ which are monoclinic, hexagonal, and orthorhombic lattice types, respectively (Luo *et al.*, 2012). The α crystal is a dominant phase which is normally found in PP products, and the β -modified crystal

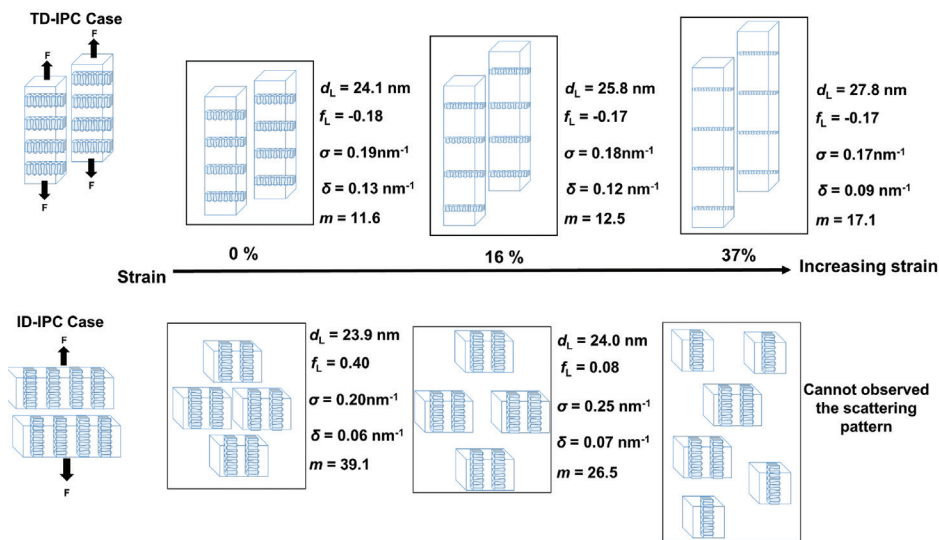


Figure 6. Proposed mechanisms for crystallite evolution of ID-IPC and TD-IPC including structural parameters at specific strain (Rungswang *et al.*)

can be induced by the β -phase NA. Luo *et al.* (2012) have reported the toughening effect of the β -phase NA of the IPC. They showed that the β -nucleated IPC performed with a significantly superior impact resistance at 0°C, while that property is not affected at 23°C and -15°C. This phenomenon can be explained by the β -phase NA possibly enhancing the chain mobility of the amorphous phase in the PP matrix which is related to the β -relaxation at about 0°C (Rungswang *et al.*, 2014).

The authors have also explored the effect of the NA type on the mechanical properties of PP by using the SAXS technique. Two types of NAs, i.e. sodium phosphate-ester salt (SPES) and 1:3,2:4-di(methylbenzylidene) sorbitol (DMBS), were used in this study.[24] SPES is an inorganic NA with a rod-like shape with its longitudinal dimension in the range of a few to hundreds of micrometers, and it is well known that SPES is a highly effective α -phase NA for

commercial use. DMBS is a sorbitol-based NA which was mentioned previously. The NAs were mixed with the PP in a twin-screw extruder at high temperature in the optimum doses. The SPES- and DMBS-nucleated PPs are abbreviated as SPES-PP and DMBS-PP, respectively. The 1-mm-thick plate specimen was prepared by injection molding for the mechanical tests and SAXS analysis. Figure 7 shows a schematic drawing of the specimen including the reference directions. The polymer melt was injected into the mold in the injected-flow direction (IFD) at high temperature before solidification by water cooling. To analyze the orientation of the crystallite, another 3 directions, i.e. injected direction (ID), normal to injected direction (ND), and transverse injected direction (TD) are needed for reference, as depicted in Figure 7. The SAXS patterns of the SPES- PP and DMBS-PP specimens in all their measured directions are shown in Figure 8. A circular pattern with accumulated arcs is

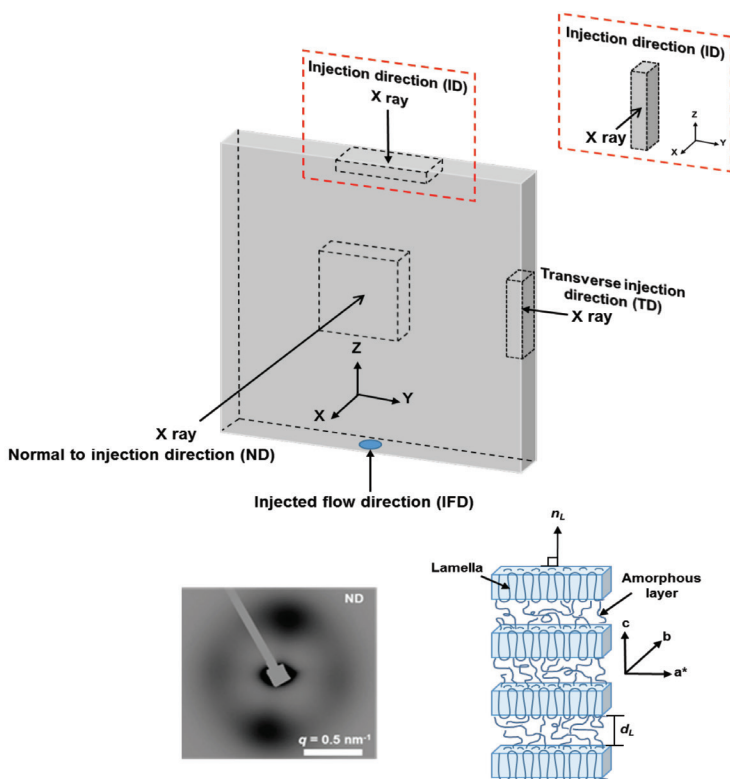


Figure 7. Schematic drawing of specimen preparation for X-ray experiments and possible model to evaluate structural parameter (Rungswang *et al.*,)

mostly found, and this indicates the preferential orientation of the lamellar crystal. The lamellar orientation can be evaluated by the full-width at the half maximum (FWHM) of the accumulated intensity of the radial-scan profile. In other word, the lower the FWHM value, the less misorientation. This indicates the higher orientation level. Table 1 shows that the FWHM values of the SPES-PP are lower than those of the DMBS-PP for the ND and the TD of which the peaks are oriented in the IFD. This suggests that the lamellae in the SPES-PP are more preferentially oriented in the IFD than the DMBS-PP. However, it is important to note that the SAXS pattern of the DMBS-PP in the ID reveals the isotropic circular pattern that implies the random orientation of the lamellae.

In the case of the SPES-PP, the accumulated intensity in the meridional and equatorial directions is observed, and this indicates the lamellar orientation.

Furthermore, to evaluate the periodically stacked structure of the lamellar crystal in depth, the mean core thickness, T_0 , the mean lamellar thickness, $\langle T \rangle$, and the long period, L , were estimated from the 1D electron density correlation function ($K(z)$) which is defined by the following Equation 7.

$$K(z) = \langle [\eta(z') - \langle \eta \rangle][\eta(z + z') - \langle \eta \rangle] \rangle$$

$$= 2 \int_0^\infty (\pi)^{-1} q^2 I(q) \cos(qz) dq \quad (7)$$

where $\langle \rangle$ is designated as the ensemble average.

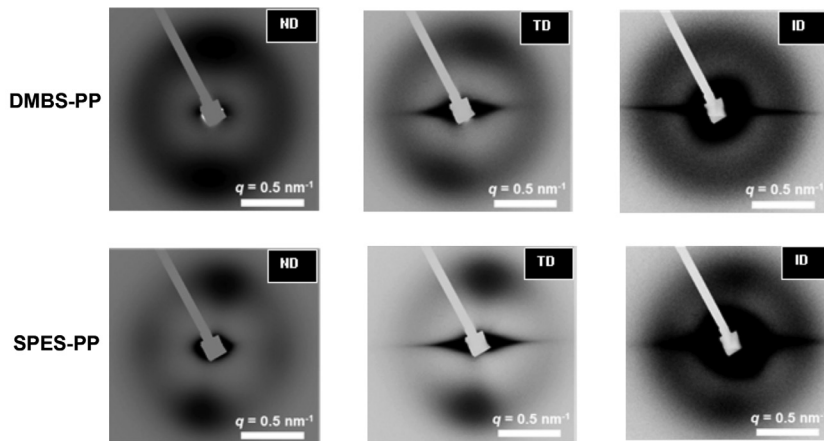


Figure 8. SAXS patterns of DMBS-PP and SPES-PP in different direction (ND, TD, and ID) (Rungswang *et al.*,)

Table 1. Structural parameters obtained from SAXS patterns of SPES-PP and DMBS-PP in ND, ID, and TD

Samples	T_0 (nm)	$\langle T \rangle$ (nm)	L (nm)	d_L (nm)	FWHM (°)
SPES-PP: ND ($\phi = 270^\circ$)	3.78	4.34	11.00	6.60	40.7
SPES-PP: ND ($\phi = 180^\circ$)	3.79	4.34	11.00	6.99	35.0
SPES-PP: ID	3.23	4.10	10.00	6.62	40.2
SPES-PP: TD	3.79	4.30	11.00	6.62	45.8
DMBS-PP: ND	3.97	4.41	11.00	6.77	48.0
DMBS-PP: ID	3.29	4.10	10.00	7.27	NA
DMBS-PP: TD	3.17	4.22	10.34	6.55	47.5

$\eta(z)$ and $\langle\eta\rangle$ are the electron density along the lamellar normal and the averaged electron density, respectively. T_0 , $\langle T \rangle$, and L are estimated from the $K(z)$, as shown in Figure 9. The results show that most of the T_0 , $\langle T \rangle$, and d_L values of the SPES-PP are smaller than those of the DMBS-PP, excepting the values in the TD. This might be due to the fast crystallization rate of the SPES-PP, and the induced numerous crystal nuclei which limit the crystal growth.

The crystal structure and its orientation are directly related to the mechanical properties, as shown in Table 2, in which the compression strength and shrinkage were tested in both the TD and ID. The compression strengths of both the SPES-PP and DMBS-PP are significantly higher in the TD than those in the ID. This suggests that the lamellae oriented parallel to the compression direction might be a reason which gives a higher compression resistance. The compression strength in the ID is higher for the DMBS-PP which might be the result of the larger $\langle T \rangle$ and d_L in the ND. For the shrinkage,

it can be observed that the shrinkages in the TD are higher than those in the ID for both the SPES-PP and DMBS-PP. This is relevant to the result that the highest degree of orientation of n_L is parallel to the ID. Thus, the chain folding, which causes the shrinkage of the crystal, is packed in the perpendicular to the n_L or TD. It is important to mention that the differences in the compressive strengths and the shrinkages for the ID and the TD are small for the DMBS-PP compared with those of the SPES-PP. This might be due to the random orientation of the lamellae in the ID in case of the DMBS-PP. This information is very useful for selecting the proper NA in a specific application to control the crystal structure in a specific use.

Conclusions

The SAXS with the intense X-ray from synchrotron radiation is a powerful technique for studying the polymer structure in depth. Used in combination with *in-situ* experiments, the structural changes

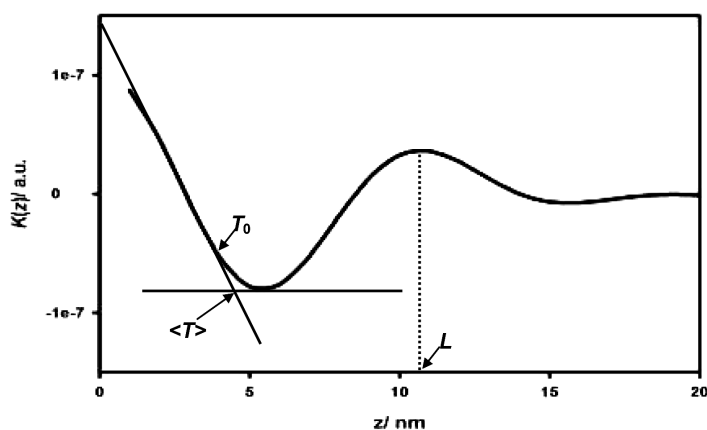


Figure 9. 1D electron density correlation function ($K(z)$) illustrating T_0 , $\langle T \rangle$, and L estimation (Rungswang)

Table 2. Compression strength and shrinkage in ID and TD of SPES-PP and DMBS-PP

Samples	Compression Strength (kPa)		Shrinkage (%)	
	ID	TD	ID	TD
SPES-PP	55.3	65.8	1.3	1.6
DMBS-PP	59.9	65.1	1.4	1.5

with the external fields can be traced, and those reveal useful information for polymer research. Some examples of the structural analyses were shown in this review, such as the isothermal treatment in the melt state and the uniaxial stretch of the specimen. Several theories and models, for example Guinier's theory and the Debye-Bueche model and correlation function, were used to evaluate the polymer structure in detail. This review aims to give an overview of the SAXS technique for analyzing polymer structures which are invariably used, especially for industrial research.

Acknowledgments

The authors would like to express their gratitude to SCG Chemicals Co., Ltd., for the financial support. The authors also would like to acknowledge Dr. Supagorn Rugmai, Dr. Siriwat Soontaranon, Dr. Prae Chirawatkul, and the staff at the Synchrotron Light Research Institute, Nakornratchasima, Thailand, who kindly facilitated the X-ray experiments.

References

- Alexander, L.E. (1969). *X-ray Diffraction Methods in Polymer Science*. Wiley-Interscience, John Wiley & Son, Inc., Toronto, ON, Canada, 582p.
- Busico, V. and Cipullo, R. (2001). Microstructure of polypropylene. *Prog. Polym. Sci.*, 26:443-533.
- Busico, V., Cipullo, R., and Segre, A.L. (2002). Advances in the ¹³C NMR characterization of ethene/propene copolymers, 1 C₂-symmetric ansa-metallocene catalysts. *Macromol. Chem. Physic.*, 203:1,403-1,412.
- Galeski, A. (2003). Strength and toughness of crystalline polymer system. *Prog. Polym. Sci.*, 28:1,643-1,699.
- Luo, F., Xu, C., Wang, K., Deng, H., Chen, F., and Fu, Q. (2012). Exploring temperature dependence of the toughening behavior of β -nucleated impact polypropylene copolymer. *Polymer*, 53(8):1,783-1,790.
- van der Meer, D.W., (2003). Structure-property relationships in isotactic polypropylene, [Ph.D. thesis]. Twente University, Enschede, The Netherlands, 203p.
- Mülhaupt, R. (2004). Hermann Staudinger and the origin of macromolecular chemistry. *Angew. Chem. Int. Edit.*, 43:1,054-1,063.
- Peacock, A.J. (2000). *Handbook of Polyethylene Structure, Properties and Application*. Marcel Dekker, Inc. New York, NY, USA, 544p.
- Piorkowska, E. and Rutledge, G.C. (2013). *Handbook of Polymer Crystallization*. John Wiley & Sons, Inc., Hoboken, NJ, USA, 482p.
- Putzig, C.L., Leugers, M.A., McKelvy, M.L., Mitchell, G.E., Nyquist, R.A., Papenfuss, R.R., and Yurga, L. (1994). Infrared spectroscopy. *Anal. Chem.*, 66:26R-66R.
- Reddy, K.R., Tashiro, K., Sakurai, S., Yamaguchi, N., Sasaki, S., Masunaga, H., and Takata, M. (2009). Isothermal crystallization behavior of isotactic polypropylene H/D blends as viewed from time-resolved FTIR and synchrotron SAXS/WAXD measurements. *Macromolecules*, 42(12):4,191-4,199.
- Roe, R. J. (2000). *Methods of X-ray and Neutron Scattering in Polymer Science*. Oxford University Press, New York, NY, USA, 352p.
- Rubinstein, M. and Colby, R.H. (2003). *Polymer Physics*. Oxford University Press, New York, NY, USA, 454p.
- Rungswang, W., Saendee, P., Thitisuk, B., Pathaweeisariyakul, T., and Cheevasrirungruang, W. (2012). Role of crystalline ethylene-propylene copolymer on mechanical properties of impact polypropylene copolymer. *J. Appl. Polym. Sci.*, 128(5):3,131-3,140.
- Rungswang, W., Plailahan, K., Saendee, P., Rugmai, S., and Cheevasrirungruang, W. (2013). Tensile deformation of in-reactor polymer alloy with preferentially oriented crystallite in parallel and perpendicular to uniaxial stretching direction: a model case from impact-resistance polypropylene copolymer. *Polymer*, 54(14):3,699-3,708.
- Rungswang, W., Thongsak, K., Prasansuklarb, A., Plailahan, K., Saendee, P., Rugmai, S., and Cheevasrirungruang, W. (2014). Effects of sodium salt and sorbitol-derivative nucleating agents on physical properties related to crystal structure and orientation of polypropylene. *Industrial and Engineering Chemistry Research*, 53(6):2,331-2,339.
- Shepard, T.A., Delsorbo, C.R., Louth, R.M., Walborn, J.L., Norman, D.A., Harvey, N.G., and Spontak, R.J. (1997). Self-organization and polyolefin nucleation efficacy of 1,3:2,4-Di-p-methylbenzylidene sorbitol. *J. Polym. Sci. Pol. Phys.*, 35:2,617-2,628.
- Stadler, F.J. and Karimkhani, V. (2011). Correlations between the characteristic rheological quantities and molecular structure of long-chain branched metallocene catalyzed polyethylenes. *Macromolecules*, 44(13):5,401-5,413.
- Stadler, F.J. and Mahmoudi, T. (2013). Evaluation of relaxation spectra of linear, short, and long-chain branched polyethylenes. *Korea-Aust. Rheol. J.*, 25(1):39-53.
- Wasanasuk, K., Tashiro, K., Hanesaka, M., Ohhara,

- T., Kurihara, K., Kuroki, R., Tamada, T., Ozeki, T., and Kanamoto, T. (2011). Crystal structure analysis of poly(l-lactic acid) α form on the basis of the 2-dimensional wide-angle synchrotron X-ray and neutron diffraction measurements. *Macromolecules*, 44(16):6,441-6,452.
- Yau, W.W. (2005). Polyolefin microstructure characterization using 3D-GPC-TREF. Proceedings of the Technical Association of the Pulp and Paper Industry (TAPPI) PLACE (Polymers, Laminations, Adhesives, Coatings & Extrusions) Conference; September 25-28, 2005; Las Vegas, NV, USA, p. 1,031-1,045.
- Zhu, H., Monrabal, B., Han, C.C., and Wang, D. (2008). Phase structure and crystallization behavior of polypropylene in-reactor alloys: insights from both inter- and intramolecular compositional heterogeneity. *Macromolecules*, 41(3):826-833.